Journal of Power Sources 477 (2020) 229029

Contents lists available at ScienceDirect

Journal of Power Sources

journal homepage: www.elsevier.com/locate/jpowsour

Modulating electrode utilization in lithium-ion cells with silicon-bearing anodes

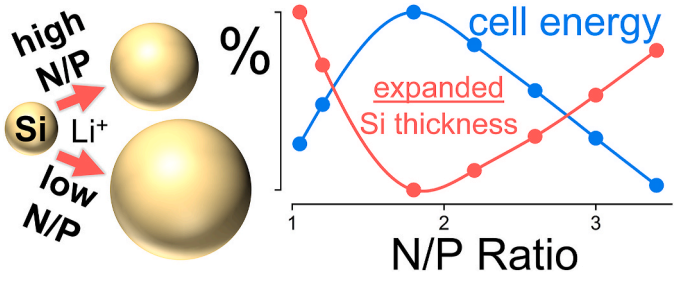
Marco-Tulio F. Rodrigues, Andressa Y.R. Prado, Stephen E. Trask, Shabbir Ahmed, Andrew N. Jansen, Daniel P. Abraham *

Chemical Sciences and Engineering Division, Argonne National Laboratory, Argonne, IL, 60439, USA

HIGHLIGHTS

- Utilization of Si capacity can be adjusted by varying the N/P ratio of full-cells.
- Higher N/P ratios will lead to partial Si utilization, lowering electrode expansion.
- Si-based cells with low N/P ratio can present rapid capacity fade.
- Increasing the N/P ratio can increase cell energy density and specific energy.

GRAPHICAL ABSTRACT



ARTICLE INFO

Keywords:
N/P ratio
Cell balancing
Capacity
Impedance
BatPaC
Dilatometry

ABSTRACT

The stability of silicon-containing anodes can, in principle, be extended by constraining these electrodes to limited states of lithiation. Partial utilization of the anode lessens the volume changes experienced by silicon particles during cycling, which can mitigate mechanisms of performance degradation. In full-cells, anode utilization can be modulated by adjusting the relative capacities of the negative and positive electrodes – the N/P ratio. Here, we examine how the N/P ratio affects the long-term stability of Si-based full-cells, and investigate how this parameter would impact the cost and energy of realistic Li-ion cells. We show that, for some configurations, cell failure due to rapid anode degradation can only by avoided at higher N/P ratios. The price of this enhanced stability is accelerated impedance rise at the cathode. Surprisingly, when electrode expansion is taken into account, increasing N/P ratio can actually increase the specific energy and energy density of silicon-rich Li-ion cells.

1. Introduction

Silicon presents high specific and volumetric capacities for lithium storage, and can potentially increase the energy delivered by Li-ion batteries (LiBs) [1,2]. The resulting Li_xSi alloys exhibit a progressive decrease in density at increasing lithium content [3], resulting in volumetric changes that approach ~300% on a particle level [4]. In practice, stresses induced by this dilation can lead to repeated fracture of Si domains, altering particle morphology and creating regions with elevated internal porosity [5], which further increases the volume expansion upon lithiation. Maintaining stable electrochemical performance in spite of these dimensional changes is key to unlocking the

* Corresponding author.
E-mail address: abraham@anl.gov (D.P. Abraham).

https://doi.org/10.1016/j.jpowsour.2020.229029
Received 9 May 2020; Received in revised form 4 September 2020; Accepted 1 October 2020
Available online 10 October 2020
0378-7753/© 2020 Elsevier B.V. All rights reserved.

benefits that Si can offer to LiB technology.

The immediate challenge posed by these structural changes is the fragmentation-induced electronic isolation of entire particle domains, which causes capacity loss by decreasing the effective amount of silicon that can engage in electrochemical reactions [2,6,7]. Even mild fragmentation of silicon particles can produce capacity fade, as the freshly exposed surfaces electro-reduce the electrolyte to form additional solid electrolyte interphase (SEI) that traps mobile Li^+ ions [8,9]. Many materials architectures have been proposed to mitigate the dimensional problems of silicon electrodes. The central idea is to craft particle structures or electrode arrangements that allow expansion to occur with minimal inter-particle stress [10]. The result is often an electrode with elevated porosity, with voids optimally distributed to accommodate the dimensional changes of silicon domains. While some of these approaches have yielded satisfactory results on a laboratory scale, manufacturing at large scale and validation at relevant loadings are still a challenge. The use of silicon nanoparticles can alleviate some of the dimensional problems that arise from repeated dilation [1]. Although advances have been reported in the research literature, these nanosilicon-based electrodes have yet to demonstrate cycling stabilities that are comparable to graphite. As a consequence, only minor amounts (<5%) of Si are added in the anode of select commercial cells, producing energy gains that are significantly smaller than what the material can theoretically deliver.

A more pragmatic approach to improve the cycle life of Si-containing cells is to limit lithiation of the silicon particles. Although these "diluted" Li_xSi alloys provide smaller capacities, they also undergo smaller dimensional changes, which translates into electrochemical longevity. This relationship between partial electrode utilization and enhanced stability has been verified by multiple research groups, by cycling silicon electrodes in cells with lithium metal (half-cells) to various lithiation cutoff potentials or capacities [11–13]. However, the silicon electrode potential (and hence the degree of lithiation) cannot be explicitly controlled in a full-cell, wherein the lithium-metal is substituted with a lithium-bearing transition metal oxide cathode that serves as the source of Li^+ ions. The full-cell voltage during cycling is the instant difference between the positive (cathode) and negative (anode) electrode potentials, which changes during cycling [7,14]; cell capacity loss progressively increases the electrode potentials that are accessed at a given voltage [7,8,15]. Nevertheless, utilization of silicon in the anode can be modulated by varying the capacity ratio between the negative and positive electrodes, which is commonly referred to as the N/P ratio [16]. Ideally, a N/P ratio close to unity minimizes excess weight in the cell, maximizing the specific energy. In practice, commercial cells have a slight excess of anode capacity to minimize the likelihood of lithium plating due to overcharge [16]. For a constant cathode, a higher N/P ratio can be achieved by utilizing anodes that have higher active material contents (typically thicker electrodes). For cells with Si electrodes charged to a fixed voltage, a higher N/P ratio would lead to higher anode potentials at the end-of-charge: the thicker anode contains a larger number of silicon particles, each being lithiated to a smaller extent.

In this study, we evaluate the practical benefits and drawbacks that elevated N/P ratios offer to cells with silicon-containing electrodes. We discuss the capacity and impedance performance of cells with 15% Si and 70% Si in the anode, at various N/P ratios. Using data from electrochemical dilatometry we highlight the effect of N/P ratios on electrode swelling. When changes in electrode dilation are considered in BatPaC models of full-cells, the use of excess anode (high N/P) can, counterintuitively, result in higher specific energy and energy density.

Additional tables and figures to amplify information contained here are included in the Supporting Information; these are referenced using the designator "S", as in Figure S1.

2. Experimental

2.1. Materials

Electrochemical tests were performed using $Li_{1.03}(Ni_{0.5}Co_{0.2}Mn_{0.3})_{0.97}O_2$ (NCM523) cathodes and Si-containing anodes. Anode formulations include both a silicon-graphite (Si-Gr) blend (15 wt% Si, 73 wt% Gr) and graphite-free electrodes (70 wt% Si), using LiPAA binder and coated on 10 μm battery grade copper foil. The silicon nanoparticles (~150 nm, 30 $m^2\ g^{-1}$ surface area), supplied by Paraclete Energy Inc., were coated with carbon (~3 wt%); the coating, in addition to improving performance, protects the silicon from hydrolysis during electrode fabrication from water-based slurries [17]. The cathodes contained 90 wt% NCM523 (Toda) and 5 wt% of both C45 and PVdF (Solvay 5130) coated on 20 μm battery grade aluminum foil. Full-cells with varying N/P ratios were constructed by combining negative and positive electrodes with different active-material loadings (see Table 1); these electrodes were fabricated at the Cell Analysis, Modeling and Prototyping (CAMP) Facility, Argonne National Laboratory (ANL). Prior to cell assembly, electrodes were vacuum-dried for 12 h at 120 °C (NCM523) or 150 °C (anodes). The coin cells (2032 format) contained 1.58 cm^2 electrodes, 2325 Celgard separator and 40 μL electrolyte (>4× excess of the total pore volume of all cell components). The electrolyte was a 1.2 mol/L solution of $LiPF_6$ in a 3:7 w/w mixture of ethylene carbonate (EC) and ethyl methyl carbonate (EMC) supplied by Tomiyama, with 10 wt% fluoroethylene carbonate (FEC, Solvay) as an additive. For dilatometry tests, the electrolyte was 1.0 mol/L LiFSI in EC: EMC 3:7 w/w (SoulBrain MI).

2.2. Electrochemical testing

Long-term cycling of *half-cells* was carried out at C/5 rate; the lithiation cutoffs varied from 0.2 V to 0 V, while delithiation was always performed to 1.0 V. Most *full-cells* were evaluated using 4.1 and 3.0 V as voltage limits for charge and discharge, respectively. A charge cutoff of 3.8 V was used in one case to achieve the desired N/P ratio. The test protocol contained multiple repetitions of 100 cycles, which included impedance measurements using a modified hybrid pulse power characterization (HPPC) test [18]. In each of these 100 cycles, cycles 1–3 are at ~ C/20 rate, 4 is a HPPC step, 5–96 are at ~ C/3 rate, 97 is a HPPC step, and 98–100 are at C/20 rate [19]. The 1C rate is defined as the current at which the full-cells are fully *discharged* in 1 h. Although multiple cells were tested for each condition, only representative data are shown here; the data were highly reproducible, as exemplified in

Table 1
Composition and physical characteristics of electrodes used in this study.

Composition	Properties
NCM523 cathode	
90 wt% $Li_{1.03}(Ni_{0.5}Co_{0.2}Mn_{0.3})_{0.97}O_2$ (Toda)	9.17 mg/cm^2 loading, 33.5% porosity, 34 μm coating
5 wt% C45 carbon (Timcal)	11.33 mg/cm^2 loading, 33.5% porosity, 42 μm coating
5 wt% PVdF binder (Solvay 5130)	18.63 mg/cm^2 loading, 35.4% porosity, 71 μm coating
Si-Gr anode	
15% Paraclete nSi/C	3.43 mg/cm^2 loading, 53.3% porosity, 39 μm coating
73 wt% MagE 3 (Hitachi)	6.21 mg/cm^2 loading, 56.4% porosity, 61 μm coating
2 wt% C45 carbon (Timcal)	
10 wt% LiPAA (LiOH titrate)	
70% Si anode	
70% Paraclete nSi/C	0.85 mg/cm^2 loading, 57% porosity, 9 μm coating
15 wt% C45 carbon (Timcal)	
15 wt% LiPAA (LiOH titrate)	

Figure S1.

2.3. Tests with harvested electrodes

To examine the state of individual electrodes after aging, the full-cells were disassembled in the discharged state in an Argon-filled glovebox. Then, the as-harvested electrodes were coupled with Li-metal to prepare half-cells. Electrode capacities were evaluated by performing two cycles at C/10, followed by a cycle at C/100. For impedance experiments, the half-cells were equilibrated at 3.9 V (oxide) or 0.125 V (silicon) for 10 h. Afterwards, half-cells containing electrodes harvested from identical full-cells were disassembled, and the appropriate electrodes were combined to form symmetric cells. Impedance spectra of symmetric cells were measured using a Solartron Analytical 1470E, after stabilizing the cells at 0 V. Spectra were collected with a 5 mV A. C. amplitude in the frequency range 10^5 to 10^{-2} Hz. In the absence of reference electrodes, symmetric cells can be used to accurately determine single-electrode impedance [20].

2.4. Electrochemical dilatometry

Dilatometry measurements were conducted using 8 mm electrode discs in a ECD-3-nano (EL-Cell GmbH) dilatometer. An electrolyte with the hydrolytically stable LiFSI salt was used to improve stability of the data; note that cells with $LiPF_6$ and LiFSI electrolytes display comparable electrochemical performance [19]. The dilatometry tests included two 30-h long "formation" cycles, in which the Si-based electrode never experienced potentials below 100 mV vs. Li/Li^+. Finally, the electrode was lithiated to 10 mV at C/25, followed by a hold at this potential for 10 h to ensure complete electrode utilization. The electrode expansion vs. capacity data shown below are from this final lithiation step. Cell delithiation was always performed to 1.0 V at the same rate as lithiation.

2.5. Techno-economic analysis

The impact of N/P ratio on the performance and cost of Li-ion cells containing Si-rich electrodes was evaluated using BatPaC version 3.1 (https://www.anl.gov/cse/batpac-model-software) [21]. BatPaC is a bottom-up model developed at ANL that is able to estimate production costs and device performance for various electrode chemistries, both at the cell and module level. The projections presented here utilize NCM622 ($LiNi_{0.6}Co_{0.2}Mn_{0.2}O_2$) as a cathode; although this material differs from the NCM523 used in the experiments, their properties and production costs are similar [22]. The model considered cells designed for deployment in 80 kW h (usable energy) packs for electric vehicles (EVs), and all projections are made assuming a 4.1 V charge cutoff. Cost comparisons are with reference to a NCM622//Gr baseline charged to 4.2 V cutoff; this baseline delivers 554.7 W h/L and 244.4 W h/kg on a cell level.

The Si-anode cells modeled here use the composition and porosity of the 70 wt% Si electrode; parameters used in the calculations are summarized in Table S1. For each N/P ratio, the volume expansion quantified in dilatometry tests is accommodated using a hypothetical conductive foam that is perfectly compressible. This foam was assumed to have the same cost and density as the separator, and an initial thickness equal to the full expansion of *all* anode layers at a given N/P ratio. Dimensional changes in other cell components were assumed to be negligible. This simplified model provides a semi-quantitative assessment of the energy gains when a silicon anode is used, instead of graphite. For cost comparisons, we assumed that the US$/kg costs of silicon nanopowders is twice that of commercially-available battery-grade graphite ($25.00 vs. $12.50 per kilogram, respectively).

3. Results and discussion

3.1. Definition of N/P ratios

Finding a consistent approach to compute N/P ratio is challenging when dealing with electrodes exhibiting sloped profiles and a wide range of areal capacities. This difficulty arises because the effective end-of-charge potential experienced by each electrode (and thus its effective capacity) after the formation cycles can vary widely. Here, we define N/P ratio as the *first delithiation areal capacity of an anode half-cell (previously lithiated to 0 V) divided by the discharge areal capacity of the first cycle of each full-cell*. This is equivalent to dividing the maximum reversible capacity of the anode by the capacity accessible in the cathode, after deducting the initial coulombic inefficiency. The N/P ratios explored here ranged from 1.3 to 3.5. The initial end-of-charge potentials at the anode for each N/P ratio were estimated by overlaying the charge areal capacity in the 3rd cycle of the full-cell with the lithiation profiles of anode half-cells.

3.2. Explaining the concept

Consider two Li-ion cells differing in their anode capacities (in mAh/cm^2), but that are otherwise identical; i.e., they have *distinct N/P ratios*. At any time, the cell voltage is defined by the difference between the potentials experienced by the cathode and the anode [14]. Below, we demonstrate that the same applied voltage will produce a different set of

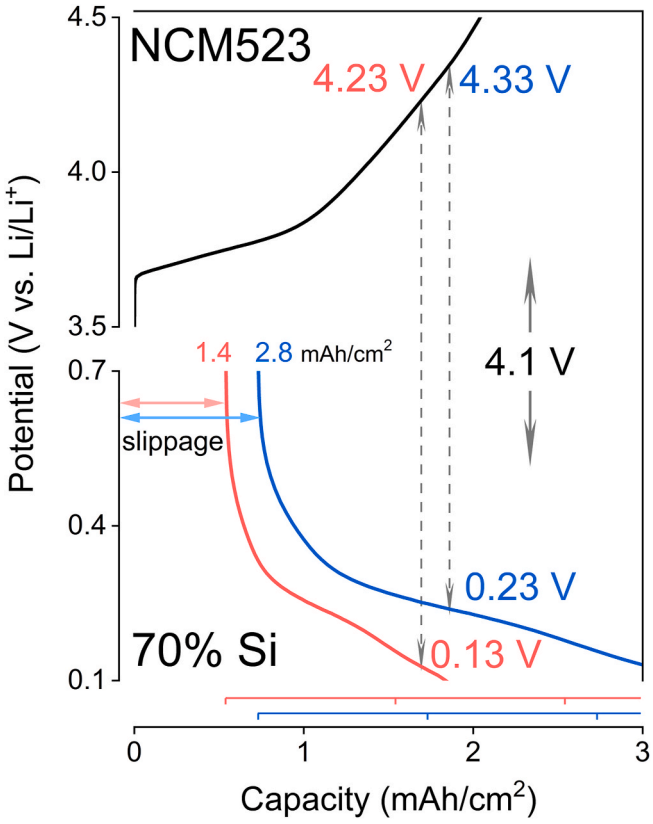


Fig. 1. Schematic showing the effect of N/P ratio on electrode potentials in a NCM523//70%Si cell. For the same cathode, doubling the anode loading (from 1.4 mA h/cm^2 in *red*, to 2.8 mA h/cm^2 in *blue*) increases the potentials experienced by both electrodes by ~100 mV. "Slippage" that results from capacity losses during formation cycling shifts the anode potentials to the right with respect to the cathode potential. Profile shown in *blue* was calculated from the one shown in *red*, while all others were obtained from half-cell tests. (For interpretation of the references to colour in this figure legend, the reader is referred to the Web version of this article.)

electrode potentials in these two cells, and discuss the multiple impacts this can have on cell performance.

Fig. 1 illustrates the case in which capacities of the 70% silicon electrodes vary by a factor of two. For the same cathode, these anodes yield cells whose N/P ratios vary by a factor of 2. The vertical distance between the cathode and anode profiles (Fig. 1) gives the voltage of the full-cell, and the capacity accessible at a given voltage can be inferred from the x-axis. When both cells are charged to 4.1 V (dashed lines), a higher N/P ratio (blue) causes both the positive and negative electrodes to experience higher potentials than when the N/P ratio is lower. That is, for the same full-cell cycling range, changing the N/P capacity ratio affects the potentials experienced by the electrodes. This potential dependence on N/P ratio is particularly large for Si-rich electrodes, as the sloped profiles magnify the effect. Fig. 1 indicates that, for a same upper cutoff cell voltage, increasing the anode loading is equivalent to constraining silicon to lower states-of-charge (SOC). As many degradation mechanisms in Si-containing electrodes correlate with dimensional changes in the particles, the N/P ratio would hence affect how the cell ages.

Electrochemical dilatometry data (Fig. 2a) show how the thickness of a 70% Si electrode varies during lithiation. Despite having an initial porosity of 57%, the composite electrode still expands 296% when the silicon is fully lithiated; the electrode pores clearly cannot fully accommodate the dilation of Si particles. If only a fraction of the silicon capacity is accessed, by confining the anode to potentials above 130 mV vs. Li/Li$^+$ (red curve in Fig. 1), the electrode expansion could be limited to 38%. Constraining the anode lithiation to 230 mV vs. Li/Li$^+$ (blue curve in Fig. 1), would further decrease the electrode expansion to 11%. The expected consequences are exemplified by the cycle life of 70% Si half-cells that are cycled with varying lithiation cutoffs (Fig. 2b). In these tests the Li counter-electrode act as a quasi-infinite source of Li$^+$ ions, and capacity fade occurs due to permanent damage in the electrode. When the silicon is cycled at full capacity (0 V) the cell degrades quickly, losing most of its capacity in the initial 50 cycles. Raising the lithiation cutoff above 100 mV vs. Li clearly minimizes the extent of irreversible damage. At 100 mV, however, the cell undergoes rapid capacity loss after 200 cycles, apparently from electrolyte depletion that results from sustained SEI formation reaction. This rapid capacity loss is not observed (and apparently delayed) when electrode lithiation is constrained to 200 mV vs. Li.

Combining all these observations, it becomes clear that electrode dilation and performance degradation of Si-containing electrodes can be regulated by controlling the N/P ratio of full-cells. Based on the two cell formulations in Fig. 1 we expect the following:

1) Cycle life – *increasing the N/P ratio could improve capacity retention*, as performance fade in Si-based cells correlates with dimensional changes. Particle "breathing" during cycling can lead to fragmentation, causing permanent loss of electrochemically-active domains. Smaller fractures created by these volume changes can also trigger electron-trapping reactions to construct a passivation layer. Both loss mechanisms should be alleviated when electrode dilation is reduced.
2) Initial coulombic efficiency – *increasing the N/P ratio will only cause a small decrease in the initial efficiency*. For the same cathode and constant cell cutoff voltage, elevating the N/P ratio consists in employing anodes with higher loadings. For a fixed electrode *composition*, this invariably results in a larger total surface area, requiring the sacrifice of more electrons to build the SEI and thus decreasing the initial coulombic efficiency. However, Fig. 1 also shows that more Li$^+$ ions are extracted from the cathode in cells with a higher N/P ratio (i.e., the cathode experiences higher potentials), which partially compensates for this higher initial loss at the anode. In addition to the injection of this extra Li$^+$ into the cell, a higher N/P ratio also reduces electrode expansion, which can minimize the effective surface area of the electrode by preventing cracks to develop in the Si particles. Thus, although a higher N/P ratio is expected to decrease the initial efficiency, this decrease is partially compensated by other mechanisms.
3) Impedance – *changing the N/P ratio can affect cell impedance* at all stages. Thicker electrodes have greater electrochemical surface areas, and thus may display lower initial impedances [23]. However, Fig. 1 shows that a higher N/P ratio leads to higher potentials at the cathode, which can accelerate impedance rise and aging of the electrode [24,25].
4) Cell capacity and energy: *a higher N/P ratio does not necessarily imply a decrease in energy density*. Increasing the N/P ratio leads to underutilization of the capacity available at Si-containing anodes, which can initially seem ineffective. Note, however, that cylindrical and prismatic cells have constant volumes, and thus electrode expansion needs to be accommodated in cell design by introducing sufficient "empty space". Otherwise, this could lead to over-compression of electrodes and separator, affecting cell performance [26]. As anode expansion is maximum at a low N/P ratio, the breathing space required by the anode could actually decrease the number of electrode layers that can be contained in the cell, lowering the energy density. Whether or not an increase in N/P ratio always decreases cell energy density depends on the electrode properties.

The above considerations inspired us to assess whether a higher N/P ratio would improve the performance retention of silicon-containing cells, and the compromises this approach would require. Experimental evaluation of these performance metrics in Si-Gr and 70% Si cells are described in the sections below.

3.3. Silicon-graphite cells

NCM523//Si-Gr cells were built with N/P ratios ranging from 1.8 to 3.5. Lower N/P ratios were deliberately avoided to limit the contribution of graphite to the overall anode capacity; under the selected cycling conditions, Si accounts for more than 2/3 of the cell capacity. Despite the differences in capacity balancing, variations in the 1st cycle

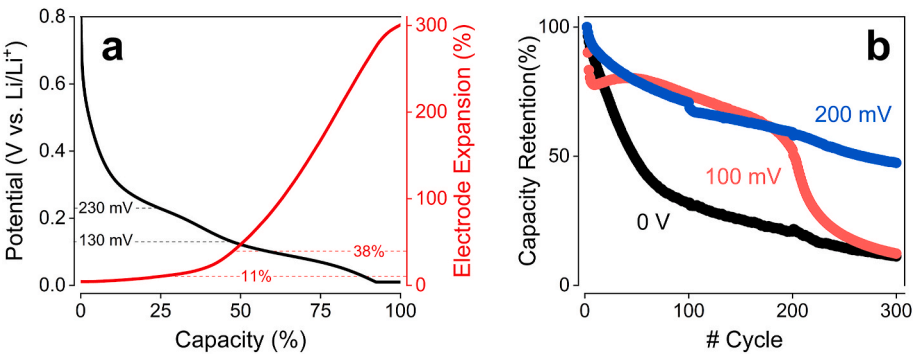


Fig. 2. Potentials and electrode longevity for a 70 wt % Si anode. (a) electrode expansion (*red*, right y-axis) and anode potentials (*black*, left axis) from electrochemical dilatometry experiments. Limiting the silicon lithiation potential can constrain electrode dilation. (b) capacity retention of half-cells lithiated to 0 (*black*), 100 mV (*red*) and 200 mV (*blue*). Accessing full capacity of the electrode leads to rapid performance loss, while higher lithiation cutoffs can slow the damage to Si particles. (For interpretation of the references to colour in this figure legend, the reader is referred to the Web version of this article.)

Table 2
Full-cells containing 15% silicon-graphite (Si-Gr) electrodes and with various N/P ratios. Coulombic efficiency is from the first cycle, while electrode potentials at the end-of-charge were estimated from the areal capacities of the full-cells and lithiation profiles of half-cells. The Si-Gr electrode expansions were estimated from dilatometry data (not shown here).

N/P ratio	Coulombic Efficiency (%)	Anode Potential (V vs. Li/Li^+)	Cathode Potential (V vs. Li/Li^+)	Estimated Electrode Expansion (%)
1.8	76.1	0.12	4.22	11%
2.8	70.1	0.20	4.30	4%
3.5	67.2	0.22	4.32	3%

coulombic efficiency were notably small (Table 2). Doubling the relative anode loading (N/P changing from 1.8 to 3.5) decreased the efficiency by ~9%. As anticipated in the previous section, this lack of variance is caused by a combination of injecting cyclable Li^+ into the cell (by exposing the cathode to higher potentials) and less expansion of the anode (by also constraining the anode to higher potentials). Approximate values of electrode potentials and anode dilation at the end-of-charge during the initial cycles are also presented in Table 2. The roughly twofold rise in the N/P ratio increased the end-of-charge anode potential by 100 mV, and decreased the overall electrode expansion by ~73%.

Fig. 3a displays the cycle life of NCM523//Si-Gr full-cells. Initial discharge capacities are similar for all systems (123–136 mA h/g), but the fade behavior varies widely. After 400 cycles, cells with a higher N/P ratio consistently exhibited improved capacity retention (Fig. 3b): ~50% of the initial active Li^+ ions were still available with N/P 3.5,

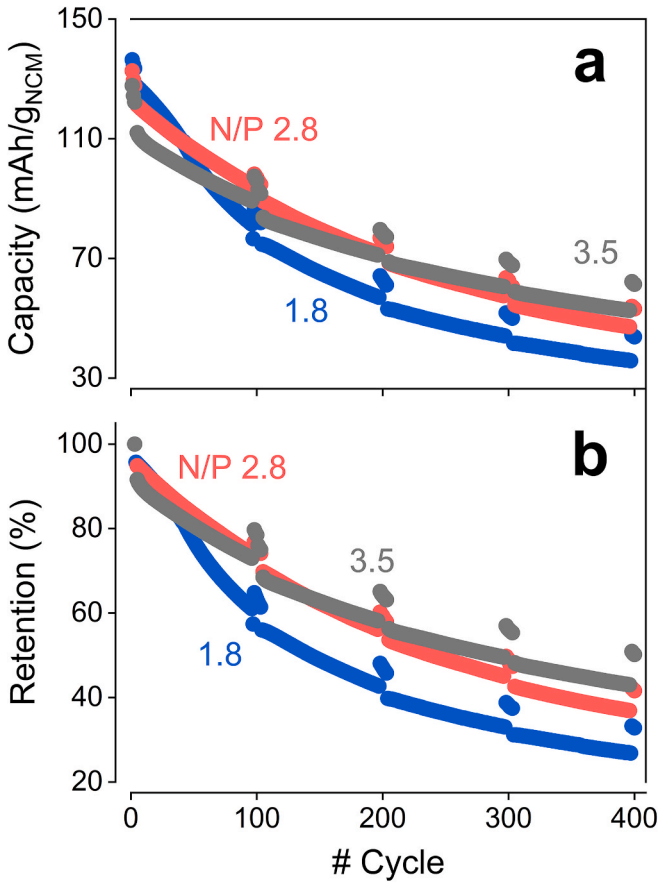


Fig. 3. (a) Discharge capacities and (b) capacity retention vs. cycle 3 for NCM523//Si-Gr cells with various N/P ratios (as marked). The data indicate that limiting Si utilization can lower the rate of capacity loss.

while only 33% remained with N/P 1.8. In all cases the *rate* of capacity loss decreased during cycling, being clearly highest in the initial 100 cycles. This is particularly true for cells with N/P 1.8, which *lost more capacity at these early stages than in the remainder of the test*. Such rapid decay does not occur for the other cells. Wetjen et al. have suggested that extensive morphological changes can occur in silicon particles within the first ~60 cycles [5]. These changes involve the transformation of initially compact nanoparticles into porous structures, causing most of the irreversible dimensional changes observed in the electrode and accelerating capacity fade. If similar transformations explain the initial behavior of cells with N/P 1.8, they are clearly not as destructive at higher N/P values. It would appear that this morphological evolution depends strongly on the utilization of the Si anode, both in nature and magnitude, and that it may be absent in cells with N/P ratios of 2.8 and above. That is, when silicon particles are only lithiated to higher potentials (lower capacities), the limited volume expansion may prevent the occurrence of significant morphological changes. As will be discussed below, analysis of anodes harvested from these full-cells indeed indicate that more electrochemically-active Si persists in systems with higher N/P ratios.

In general, the results in Fig. 3 support our hypothesis that *limiting the utilization of silicon particles can restrain the mechanisms of capacity fade*. At early stages of cycling, maintaining Si at higher potentials can avoid transformations that lead to dramatic Li^+ loss. Additionally, capacity fade tends to increase graphite's contribution to the anode capacity [15], justifying the varying rates of fade over cycling. In contrast, full-cells containing Si-free, graphite anodes typically show a linear capacity fade over cycling [27].

While capacity fade in graphite cells stems mostly from Li^+ trapping at the SEI, silicon-based systems can undergo significant permanent damage. The half-cell data presented in Fig. 2b show that the extent of this damage can be modulated by adjusting the range of potentials to which the electrode is exposed. To verify how these previous observations translate to anodes in the full-cells, we disassembled the samples discussed in Fig. 3, harvested the cathodes and anodes, and used them to build half-cells. Fig. 4 shows the cycling profiles of these half-cells at a C/100 rate; at such low currents, residual electrode capacity can be determined as impedance effects are negligible. At 100 mV vs. Li/Li^+, a pristine Si-Gr electrode can deliver 504 mA h/g, where "g" includes the weight of Si and carbons in the electrode (Fig. 4a); after 400 cycles at N/P 3.5, the anode can still provide 87% of this capacity, which is higher than the 70% exhibited by the anode from N/P 2.8. Half-cells built with harvested cathodes, on the other hand, show no capacity loss, regardless of the original N/P ratio (Fig. 4b). This shows that *a higher N/P ratio assists in preserving the electrochemical activity of silicon particles*, with no permanent loss of Li^+ sites at the cathode.

The capacity-retention gains discussed above are partially negated by the accelerated impedance rise at higher N/P ratios. Fig. 5a displays the evolution of the area-specific impedance (ASI) of full-cells with different N/P ratios during the tests shown in Fig. 3. The ASI values were obtained from 10-s-long 3C discharge pulses at ~3.8 V; the ASI has little variance with state-of-charge around this voltage [18], making it appropriate to track impedance evolution during aging. Although the initial impedance is similar in both systems, the impedance increases faster for the higher N/P ratio, being ~18% higher after 400 cycles. To verify the sources of impedance rise, symmetric cells were assembled from electrodes harvested from cells with N/P of 2.8. Before building the symmetric cells, the electrodes were cycled in half-cells, and finally equilibrated at 125 mV (for Si-Gr) or 3.9 V (for NCM523). Symmetric cells containing pristine electrodes (that only experienced formation cycles) were also built. Fig. 5b–c shows EIS spectra for the anode and cathode symmetric cells, respectively. Changes in the Si-Gr impedance as a result of cycling are minimal, while the cathode impedance is doubled. This observation is in agreement with our previous work, showing that impedance rise over aging comes mostly from the cathode, both in graphite and Si-Gr systems [7,27]. This also confirms that the

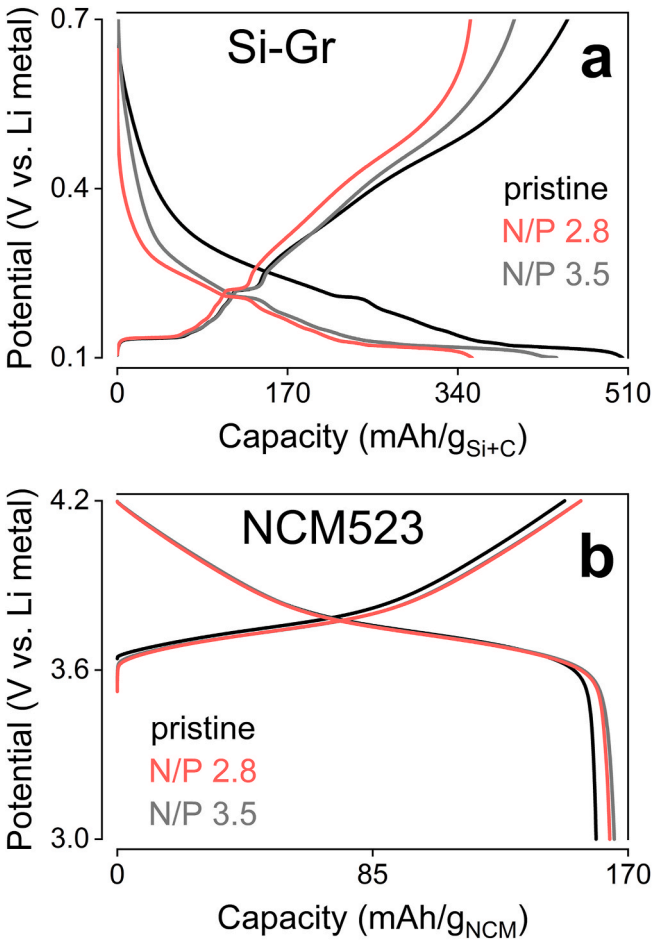


Fig. 4. Half-cell profiles of electrodes harvested from full-cells with various N/P ratios after 400 cycles: (a) Si-Gr; (b) NCM523. The data were acquired at a C/100 rate to minimize impedance effects on the measured electrode capacity. A higher N/P ratio preserves integrity of the Si-Gr electrode, but has negligible effect on cathode stability.

ASI increases in Fig. 5a occur at the cathode, and that a higher N/P ratio indeed leads to faster aging of the positive electrode.

In summary, these experiments with Si-Gr electrodes demonstrate that full-cells with a higher N/P ratio have a lower rate of capacity fade, with only a moderate decrease in initial coulombic efficiency. This is partly due to the higher potentials experienced by the silicon at high N/P ratios, which are less damaging to the particles. However, the oxide cathode is exposed to potentials that are proportionally higher, accelerating impedance rise.

3.4. 70% Si cells

Table 3 shows the general characteristics of NCM523//Si cells (with 70 wt% Si in the anode) with various N/P ratios. As for the Si-Gr cells, the initial coulombic efficiency only decreased by 7% on increasing the N/P ratio from 1.3 to 2.9. This is particularly remarkable for these Si-rich electrodes, which contain 85 wt% of nanoparticles (silicon + carbon) and thus present high surface areas. Also of note is the dramatic decrease in the projected electrode expansion at higher N/P ratios. This variation is caused by the steeper slope of the dilation curve as the electrode experience potentials below ~150 mV vs. Li/Li$^+$ (Fig. 2a), exemplifying the magnitude by which N/P ratio can regulate the dimensional changes of Si-rich anodes.

The cycle life of these Si-rich cells is exhibited in Fig. 6. The cell with N/P 1.3 shows rapid capacity fade. Some of this charge loss results from

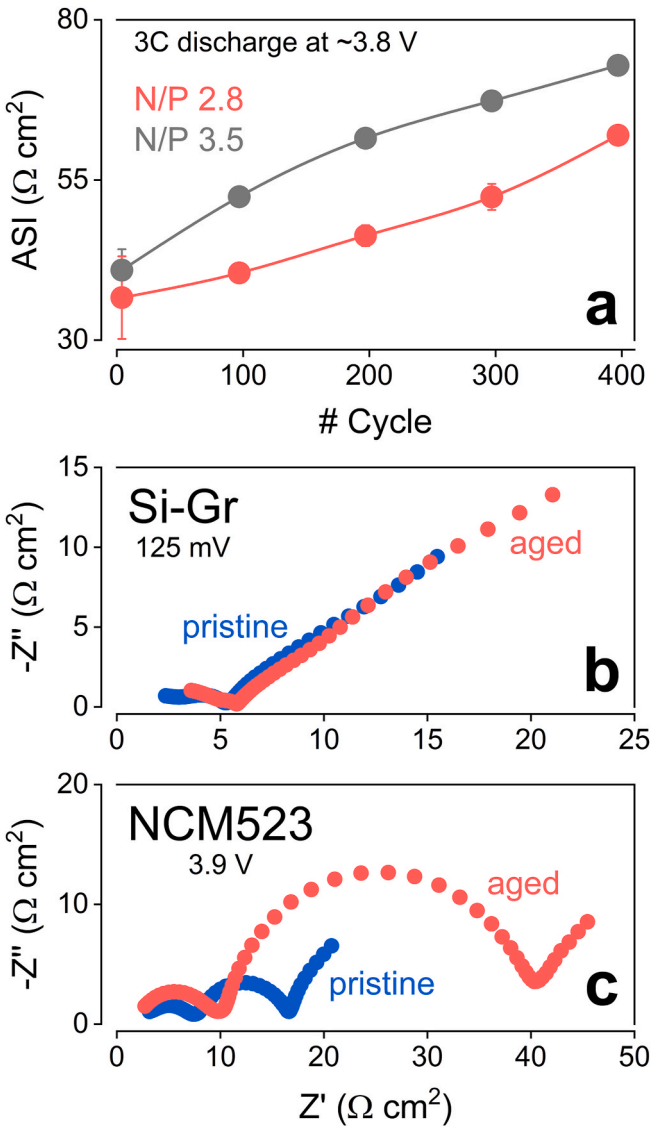


Fig. 5. N/P ratio and impedance in Si-Gr full-cells: a) evolution of the area-specific impedances (ASI) of cells with different N/P ratios. Impedance spectra of symmetric cells containing cycled and pristine Si-Gr (b) and NCM523 (c) electrodes. A higher N/P ratio exposes the cathode to higher potentials, accelerating impedance rise.

Table 3
Full-cells containing 70 wt% Si electrodes and with various N/P ratios. Coulombic efficiency is from the first cycle, while electrode potentials were estimated from areal capacities of the full-cells and lithiation profiles of half-cells. Electrode expansions were estimated from the dilatometry data in Fig. 2a.

N/P ratio	Coulombic Efficiency (%)	Anode Potential (V vs. Li/Li$^+$)	Cathode Potential (V vs. Li/Li$^+$)	Estimated Electrode Expansion (%)
1.3	74.1	0.05	4.15	225%
1.7	71.4	0.10	4.20	92%
2.4	67.2	0.16	4.26	24%
2.9	67.0	0.20	4.00[a]	15%

[a] This full-cell was charged to 3.8 V

silicon particle damage and coating delamination (Fig. 2c); in addition, we noted the presence of *plated Li* using Raman spectroscopy [28] (Figure S2). At high levels of anode utilization, the permanent deactivation of Si sites occurs faster than Li$^+$ trapping at the SEI, leading to

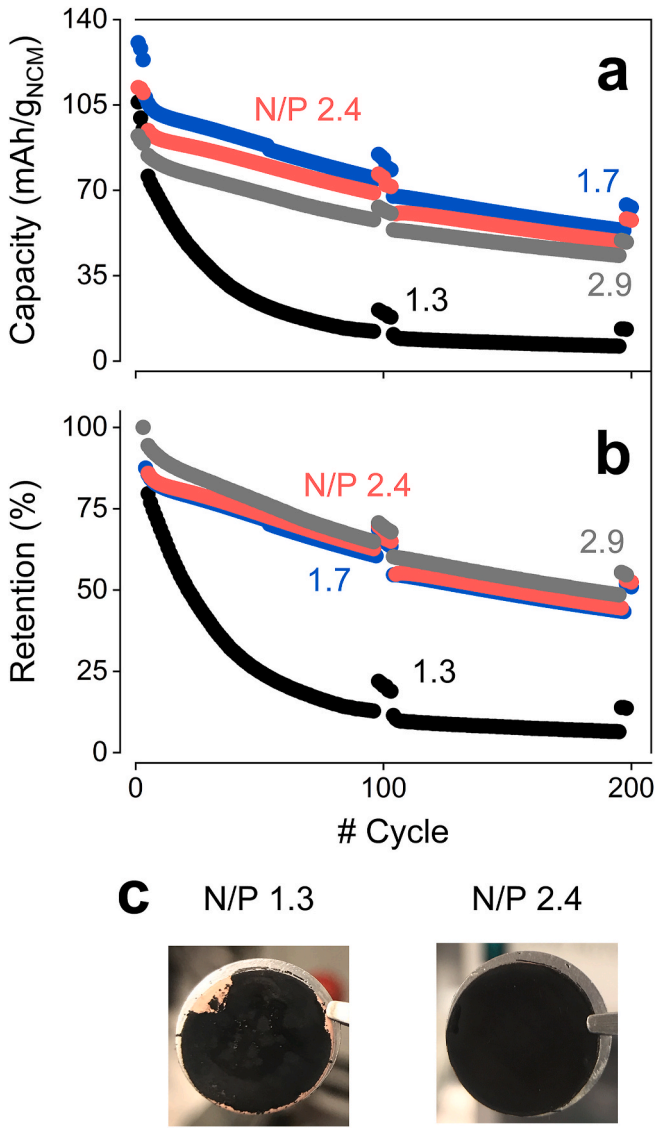


Fig. 6. The effect of N/P ratio on NCM523 full-cells *versus* 70 wt% Si: a) discharge capacities. b) capacity retention vs. cycle 3. c) photograph of electrodes harvested from cells with low (1.3) and high (2.4) N/P ratios after 200 cycles. Avoiding low N/P ratios can prolong cycle life and avoid delamination of the negative electrode.

overcharge of the cell even at an N/P ≫ 1. Curiously, the remaining cells (N/P 1.7, 2.4, 2.9) showed very little difference in cycle life, with all of them retaining ~55% of their initial capacity after 200 cycles. This is in striking contrast with the Si-Gr cells (Fig. 3), in which capacity retention improved up to ~15% at higher N/P values. Analysis of the data suggests that this difference stems from variations in the effective potentials experienced by the silicon electrodes during the experiments. Capacity loss leads to shifts in the relative alignment of electrode potentials, causing both cathode and anode to experience progressively higher potentials [15]. For the 70% Si cells (Fig. 6), Li^+ loss will steer the anode away from further degradation. The estimated anode potentials during cycling of these cells is displayed in Figure S3a. While the initial potentials of cells with N/P ratios 2.4 and 2.9 are very distinct, impedance effects decrease the capacity of the former at C/3, making these systems nearly identical. Hence, they both experience similar potentials that are higher than 200 mV vs. Li/Li^+ for most of the test. In the case of N/P 1.7, the end-of-charge potentials quickly move away from its initial value, reaching ~160 mV vs. Li/Li^+ after only 20 cycles. Consulting Fig. 2a and Table 3, it is clear that this drift suffices to reduce the projected electrode expansion from 92% to 24%. All in all, although these 70% Si cells with varying N/P ratios experience different *initial* conditions, they eventually approach a similar state due to capacity fade. In contrast, in *Si-Gr systems* (Fig. 3) LiC_x compounds can only be formed at specific potentials [14,29], exposing the Si particles that remain active to high SOCs for longer than they would experience in Gr-free cells, exacerbating differences caused by N/P ratios (Fig. S4).

Consulting Fig. 2b, it is clear that the half-cell that is lithiated to 200 mV permanently loses ~40% of its capacity after 200 cycles. With that in mind, the capacity retention of the 70% Si full-cells upon extended cycling (Fig. 6) is apparently limited by the integrity of the Si electrodes used in this study. We also note that the effect of N/P ratio on cell impedance is less clear in these Si-rich full-cells, as the anode can also contribute to ASI rise; these effects can be elucidated with 3-electrode tests, to be discussed in a future publication.

3.5. Cost and performance considerations

The discussion above clearly indicates that avoiding low N/P ratios can extend the cycle life of Si-containing cells. However, to estimate the energy gains offered by silicon to Li-ion cells, we need to account for the *effective anode volume* at the end-of-charge. A lack of extra volume in the cell into which the silicon electrode can dilate could lead to compression of the separator, thereby affecting its transport properties [26,30]. Here, we utilize the thickness changes measured by electrochemical dilatometry to estimate the effective anode volume as a function of the N/P ratio.

BatPaC was used to model the effect of N/P ratio on the projected cost and performance metrics when accommodating electrode expansion. The model considered the assembly of a battery pack with 80 kW h of usable energy, using four hundred 68.3 Ah prismatic cells. The cathode and cell thicknesses were maintained constant at 102.8 μm and ~20 mm, respectively, while the lateral dimensions of the cell case were allowed to vary to meet the capacity target. Cell-level projections from BatPaC are displayed in Fig. 7. For an ideal, isovolumetric electrode, increasing the N/P ratio would cause a quasi-linear decrease in energy density and specific energy (shown in gray in Fig. 7a–b). Si-rich electrodes are, however, *not* isovolumetric, expanding and contracting during lithiation and delithiation, respectively. Fig. 7a shows that for a cell design in which *all* the intrinsic anode expansion can be accommodated (i.e., the added "empty" space equals the expansion estimated from our dilatometry tests; shown in dark blue), the energy metrics are *maximum* at N/P ~1.8. The "breathing space" added to the cells with lower N/P ratios decreases the number of electrode layers that can be packed into the cell (Figure S5a), requiring each layer to be longer and wider to achieve 68.3 Ah. The resulting changes in case dimension at low N/P ratios affects the energy values in Fig. 7a–b, as the cells would present a higher total volume and weight. Hence, *for electrodes that undergo severe expansion, a low N/P ratio can actually be detrimental to energy metrics*.

In practice, the volume accommodation required by Si-based electrodes may differ from the values measured by electrochemical dilatometry, for two main reasons. One is that the magnitude of electrode dilation in the cell may be affected by the mechanical load exerted by the cell stack; i.e., the electrode actually expands against a larger opposing force than in our tests. The second is that some level of mechanical load may be *allowed* to develop in the cell stack. These scenarios were modeled by assuming a maximum effective electrode expansion of half, a third and a sixth of what was measured in the dilatometry tests, while maintaining the same *relative* dependence of dilation *versus* SOC. That is, in these hypothetical cases the dilation curve in Fig. 2a was downscaled by the appropriate amount. These projected scenarios are also included in Fig. 7. As the accommodated maximum expansion decreases to 1/3 of the experimental value, there is very little difference between the expected energies for cells with N/P ratios ranging from 1.05 to 1.8; changing the N/P ratio would have little effect on energy metrics. With

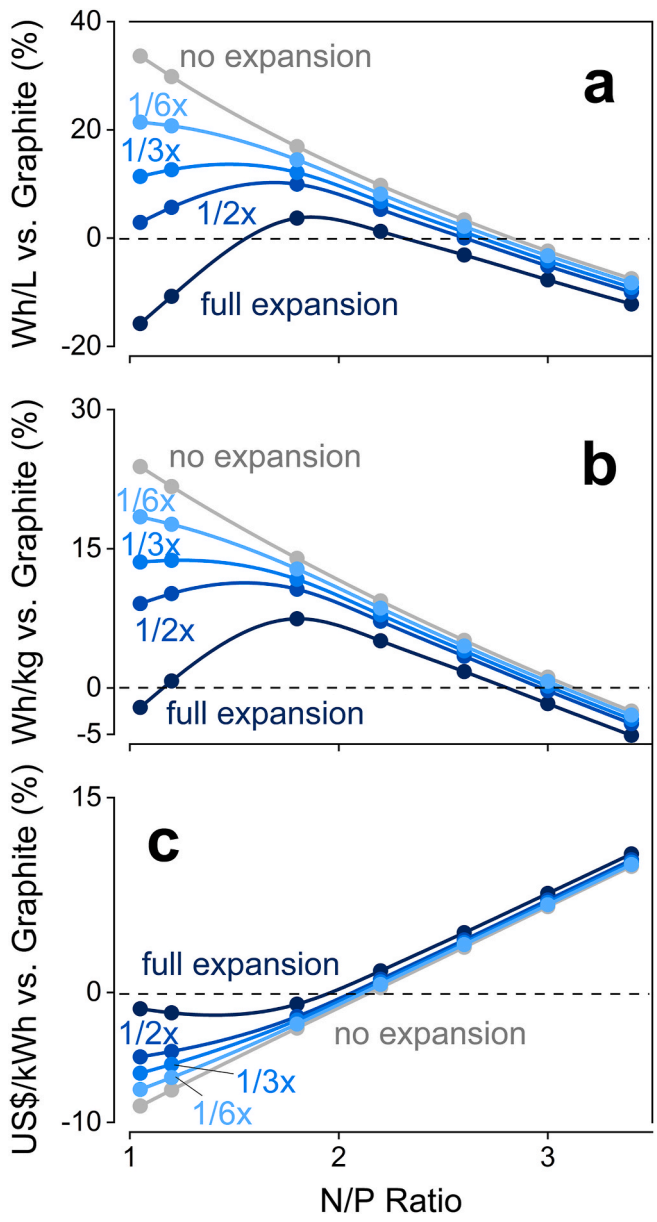


Fig. 7. Techno-economic analysis of the effect of N/P ratio on cell metrics for anodes with 70% Si, compared to a graphite-based baseline: a) gains in energy density. b) gains in specific energy. c) cost. For high levels of expansion, a moderate N/P ratio (~1.8) yields the highest energy figures. The model considered cases in which the electrode dilation accommodated by the cell design equaled the measured in dilatometry experiments ("full expansion"), or was half, a third or a sixth of that value.

an additional downscale in dilation to 1/6 of experimental values, an N/P ratio closer to unity finally becomes more advantageous (light blue). Nevertheless, the tradeoff in specific energy for operating at moderate N/P ratio would only be ~6%, much smaller than in the case of isovolumetric electrodes. The observation that, in many scenarios, *a moderate N/P ratio can still deliver elevated energy density and/or specific energy gains* offers great design flexibility for battery manufacturers exploring N/P as a variable.

Fig. 7 is also sobering in showing that electrode expansion can counteract the benefits that silicon brings to Li-ion batteries. For highly dilating electrodes, as the ones investigated in the present work, full accommodation of expansion would lead to barely any gains in energy density. However, we remind the reader that the electrodes used in this study are far from optimal; decreasing electrode porosity or increasing the effective capacity provided by silicon particles could boost the improvements offered by silicon (Figure S5b,c).

If silicon can be manufactured at low enough costs, Si-rich cells with moderate N/P ratios can still be cheaper than the current graphite-based technology (Fig. 7c). Interestingly, when the full electrode expansion is accommodated by the design, the cells with N/P of 1.05 become more expensive due to the costs associated with fabricating longer and wider cases. This effect disappears for the other projections. For lower expansions (1/2, 1/3 and 1/6× in Fig. 7c), increasing the N/P ratio from 1.05 to 1.8 would increase the cell cost by only ~5%, while still maintaining it below the cost to manufacture the baseline graphite cells.

3.6. Scholium

We are aware of recent reports that explore the effect of N/P ratios on Si-based cells. The size, shape and ordering of the silicon particles vary widely in these studies, creating an opportunity to infer general trends on the effect of electrode capacity balancing. For example, Reuter et al. report negligible changes in NCM811//Si cell performance when the N/P ratio was varied in the 1.15–2.70 range [31]. Their anode comprised amorphous columnar silicon thin films, structured to accommodate some of the lateral electrode dilation during lithiation. Baasner et al. explored N/P ratios of 0.8–3.2 in NCM111 full-cells containing a variety of silicon-based anodes, including columnar Si thin films, silicon nanowires and silicon-carbon composites [32]. In all cases, partial utilization of the anode improved capacity retention, though stability gains were apparently minimal for composite electrodes. Jantke et al. conducted similar studies using composite electrodes with micron-sized silicon particles in NCM622 full-cells [33]. For 4.5 μm Si particles, a decrease in anode utilization produced a monotonic increase in capacity retention; the gains diminished for smaller (0.8 μm) particles. In their study, low N/P ratios were not investigated, as the large particles could not accommodate higher states of lithiation without undergoing significant damage.

In the light of these reports, and the findings of our study, it becomes clear that the effect of N/P ratio is highly dependent on the Si electrodes being investigated. In certain cases, limiting Si utilization is an *essential* requirement to achieve an operational cell. In other cases, electrode architecture may be able to disperse the strains that develop along Si domains during lithiation, alleviating the problems that we observed at lower N/P ratios. With these considerations in mind, the analyses summarized in Fig. 7 are vital to evaluate the true impact of N/P ratios on energy metrics. Even when an increase in N/P ratio does not produce appreciable gains in cell *stability*, changes in design dictated by electrode expansion can render these approaches not only practical, but also advantageous. We believe that the *qualitative* behavior of the curves in Fig. 7 are general, given that the rate of electrode dilation becomes much greater at higher states of lithiation. In fact, such behavior appears to be pervasive in the literature reporting dilatometry tests of Si-rich electrodes [4,34]. The required corrections imposed by expansion will naturally depend on the magnitude of the dilation. Several analytical techniques accessible to academic laboratories and cell manufacturers are capable of estimating electrode expansion, which can inform models (such as BatPaC) that project the effects of cell configuration on cost and performance.

4. Conclusions

Dimensional changes that accompany the formation of Li–Si alloys offer significant challenges to stable cycling. As this lithiation-induced dilation is greater at higher states-of-charge, it can be modulated by limiting the utilization of Si-based anodes. Our experiments with half-cells containing 70 wt% Si anodes that were lithiated to different cut-off potentials show that the effects on capacity retention can be significant. When the entire capacity of silicon is used, performance degrades quickly due to irreversible damage in the electrode, but this catastrophic

failure can be curtailed by constraining the Si electrode to operate at higher potentials.

Anode potential control in full-cells can be achieved by adjusting the N/P ratio. For a fixed cathode and charge cutoff voltage, higher-loading anodes can limit the utilization of silicon. In our 70% Si full-cells, a N/P ratio of 1.3 led to poor cycling stability, while nearly identical improved performance was achieved for N/P ratios between 1.7 and 2.9. In contrast to half-cells, in which the minimum anode potential is explicitly fixed, potential shifts caused by capacity loss constantly alters the extent to which Si particles are lithiated in a full-cell. These shifts may explain why performance varied little in our cells above a certain capacity balancing threshold. In tests with 15%Si-Gr anodes, in which capacity is preserved longer and electrode potentials are "pinned" by the graphitic plateaus, differences in cell stability with varying N/P ratios were more apparent. All in all, our studies indicate that avoiding high lithiation-levels can be vital to the stability of Si-based cells.

Although it may seem reasonable to assume that partial anode utilization would decrease specific energy and energy density of the cell, this is not necessarily true when electrode dilation is taken into account. Our techno-economic analysis shows that for certain levels of dilation, *a moderate N/P ratio could actually lead to higher energy figures* than if the relative electrode capacities were closer to unity. The severe expansion in anodes operating at low N/P ratios magnifies the *effective volume* that these electrodes occupy in the cell. Accommodating these dimensional changes thus decreases the number of electrode layers that can be packed within a given cell format, lowering the achievable energy. This counterintuitive result indicates that, when Si-rich anodes are used, the N/P ratio parameter should be optimized during the design of high energy cells.

Nevertheless, there are compromises to be made when building cells with excess anode capacity. A higher N/P ratio will expose the cathode to higher potentials, which can accelerate impedance rise at this electrode. This is a particular concern for cathodes containing certain oxides, which are susceptible to oxygen loss and the subsequent surface reconstruction [35]. In these cases, higher N/P ratios would possibly require the cell to be operated at lower voltages, which would lessen the energy gains. Another concern is that the anode surface area increase which accompanies an increase in N/P ratio will magnify the amount of charge that is lost to SEI formation. Fortunately, this concern is mitigated by the limited anode expansion and the higher cathode potentials (as more Li^+ are extracted from this electrode); anode prelithiation can also be used to alleviate this problem [15,36].

The discussions here highlight the importance of considering the N/P ratio when conducting academic research with Si-based full-cells. Electrode capacity balancing must be considered during experiment design and reported to contextualize the findings. It is also important to account for irregularities in the electrode coating, which are common in hand-made, laboratory-scale electrodes. Local variations in silicon-loading can artificially alter the N/P ratio of full-cells, making it difficult to achieve consistent and reproducible results.

CRediT authorship contribution statement

Marco-Tulio F. Rodrigues: Experiment . **Andressa Y.R. Prado:** Electrochemical Dilatometry. **Stephen E. Trask:** Electrode Fabrication. **Shabbir Ahmed:** BatPaC Modeling & Analysis. **Andrew N. Jansen:** Supervision, and . **Daniel P. Abraham:** Conceptualization, Writing - review & editing.

Declaration of competing interest

The authors declare that they have no known competing financial interests or personal relationships that could have appeared to influence the work reported in this paper.

Acknowledgements

We gratefully acknowledge support from the Vehicle Technologies Office, (VTO) at the U.S. Department of Energy (DOE). The electrodes were fabricated at DOE's CAMP (Cell Analysis, Modeling and Prototyping) Facility, Argonne National Laboratory. The CAMP Facility is fully supported by DOE-VTO. We are grateful to our many Argonne colleagues, especially Joseph Kubal, Alison Dunlop, Bryant Polzin, Ilya Shkrob and Dennis Dees, for their support during this effort. The submitted manuscript has been created by UChicago Argonne, LLC, Operator of Argonne National Laboratory ("Argonne"). Argonne, a U.S. Department of Energy Office of Science laboratory, is operated under Contract No. DE-AC02-06CH11357. The U.S. Government retains for itself, and others acting on its behalf, a paid-up nonexclusive, irrevocable worldwide license in said article to reproduce, prepare derivative works, distribute copies to the public, and perform publicly and display publicly, by or on behalf of the Government.

Appendix A. Supplementary data

Supplementary data to this article can be found online at https://doi.org/10.1016/j.jpowsour.2020.229029.

References

[1] M.N. Obrovac, V.L. Chevrier, Chem. Rev. 114 (2014) 11444–11502.
[2] S. Chae, M. Ko, K. Kim, K. Ahn, J. Cho, Joule 1 (2017) 47–60.
[3] H. Kim, C.-Y. Chou, J.G. Ekerdt, G.S. Hwang, J. Phys. Chem. C 115 (2011) 2514–2521.
[4] D.Y.W. Yu, M. Zhao, H.E. Hoster, ChemElectroChem 2 (2015) 1090–1095.
[5] M. Wetjen, S. Solchenbach, D. Pritzl, J. Hou, V. Tileli, H.A. Gasteiger, J. Electrochem. Soc. 165 (2018) A1503–A1514.
[6] S. Komaba, N. Yabuuchi, T. Ozeki, Z.-J. Han, K. Shimomura, H. Yui, Y. Katayama, T. Miura, J. Phys. Chem. C 116 (2012) 1380–1389.
[7] M. Klett, J.A. Gilbert, S.E. Trask, B.J. Polzin, A.N. Jansen, D.W. Dees, D. P. Abraham, J. Electrochem. Soc. 163 (2016) A875–A887.
[8] K. Kalaga, M.-T.F. Rodrigues, S.E. Trask, I.A. Shkrob, D.P. Abraham, Electrochim. Acta 280 (2018) 221–228.
[9] R. Kumar, A. Tokranov, B.W. Sheldon, X. Xiao, Z. Huang, C. Li, T. Mueller, ACS Energy Lett. 1 (2016) 689–697.
[10] M. Piwko, T. Kuntze, S. Winkler, S. Straach, P. Härtel, H. Althues, S. Kaskel, J. Power Sources 351 (2017) 183–191.
[11] N. Dimov, K. Fukuda, T. Umeno, S. Kugino, M. Yoshio, J. Power Sources 114 (2003) 88–95.
[12] K. Kierzek, J. Machnikowski, Electrochim. Acta 192 (2016) 475–481.
[13] B. Laïk, D. Ung, A. Caillard, C. Sorin Cojocaru, D. Pribat, J.-P. Pereira-Ramos, J. Solid State Electrochem. 14 (2010) 1835–1839.
[14] M.-T.F. Rodrigues, K. Kalaga, S.E. Trask, D.W. Dees, I.A. Shkrob, D.P. Abraham, J. Electrochem. Soc. 166 (2019) A996–A1003.
[15] M.-T.F. Rodrigues, J.A. Gilbert, K. Kalaga, D.P. Abraham, J. Phys.: Energy 2 (2020), 024002.
[16] J. Kasnatscheew, T. Placke, B. Streipert, S. Rothermel, R. Wagner, P. Meister, I. C. Laskovic, M. Winter, J. Electrochem. Soc. 164 (2017) A2479–A2486.
[17] M.-T.F. Rodrigues, S.E. Trask, I.A. Shkrob, D.P. Abraham, J. Power Sources 395 (2018) 289–294.
[18] D.P. Abraham, S.D. Poppen, A.N. Jansen, J. Liu, D.W. Dees, Electrochim. Acta 49 (2004) 4763–4775.
[19] S.E. Trask, K.Z. Pupek, J.A. Gilbert, M. Klett, B.J. Polzin, A.N. Jansen, D. P. Abraham, J. Electrochem. Soc. 163 (2015) A345–A350.
[20] C. Bünzli, H. Kaiser, P. Novák, J. Electrochem. Soc. 162 (2014) A218–A222.
[21] P.A. Nelson, S. Ahmed, K.G. Gallagher, D.W. Dees, in: Modeling the Performance and Cost of Lithium-Ion Batteries for Electric-Drive Vehicles, third ed., Argonne National Lab. (ANL), Argonne, IL (United States), 2019, p. 130 (Report ANL/CSE-19/2).
[22] S. Ahmed, S.E. Trask, D.W. Dees, P.A. Nelson, W. Lu, A.R. Dunlop, B.J. Polzin, A. N. Jansen, J. Power Sources 403 (2018) 56–65.
[23] W. Lu, A. Jansen, D. Dees, P. Nelson, N.R. Veselka, G. Henriksen, J. Power Sources 196 (2011) 1537–1540.
[24] J.A. Gilbert, I.A. Shkrob, D.P. Abraham, J. Electrochem. Soc. 164 (2017) A389–A399.
[25] M.-T.F. Rodrigues, K. Kalaga, S.E. Trask, I.A. Shkrob, D.P. Abraham, J. Electrochem. Soc. 165 (2018) A1697–A1705.
[26] J. Cannarella, C.B. Arnold, J. Power Sources 245 (2014) 745–751.
[27] J.A. Gilbert, J. Bareño, T. Spila, S.E. Trask, D.J. Miller, B.J. Polzin, A.N. Jansen, D. P. Abraham, J. Electrochem. Soc. 164 (2016) A6054–A6065.
[28] M.-T. Fonseca Rodrigues, V.A. Maroni, D.J. Gosztola, K.P.C. Yao, K. Kalaga, I. A. Shkrob, D.P. Abraham, ACS Appl. Energy Mater. 2 (2019) 873–881.

[29] K.P.C. Yao, J.S. Okasinski, K. Kalaga, J.D. Almer, D.P. Abraham, Adv. Energy Mater. 9 (2019) 1803380.
[30] M.F. Lagadec, R. Zahn, V. Wood, J. Electrochem. Soc. 165 (2018) A1829–A1836.
[31] F. Reuter, A. Baasner, J. Pampel, M. Piwko, S. Dörfler, H. Althues, S. Kaskel, J. Electrochem. Soc. 166 (2019) A3265–A3271.
[32] A. Baasner, F. Reuter, M. Seidel, A. Krause, E. Pflug, P. Härtel, S. Dörfler, T. Abendroth, H. Althues, S. Kaskel, J. Electrochem. Soc. 167 (2020), 020516.
[33] D. Jantke, R. Bernhard, E. Hanelt, T. Buhrmester, J. Pfeiffer, S. Haufe, J. Electrochem. Soc. 166 (2019) A3881–A3885.
[34] T. Kim, S. Park, S.M. Oh, J. Electrochem. Soc. 154 (2007) A1112.
[35] R. Jung, M. Metzger, F. Maglia, C. Stinner, H.A. Gasteiger, J. Electrochem. Soc. 164 (2017) A1361–A1377.
[36] L. Zhang, W.M. Dose, A.D. Vu, C.S. Johnson, W. Lu, J. Power Sources 400 (2018) 549–555.